Monthly Notices of the ROYAL ASTRONOMICAL SOCIETY
MNRAS **451,** 3210–3218 (2015) doi:10.1093/mnras/stv1117

Redshifted diffuse interstellar bands in the Orion OB1 association

J. Krełowski,[1⋆] G. A. Galazutdinov,[2,3] G. Mulas,[4⋆] M. Maszewska[1] and C. Cecchi-Pestellini[5⋆]

[1]*Center for Astronomy, Nicholas Copernicus University, Gagarina 11, Pl-87-100 Toruń, Poland*
[2]*Instituto de Astronomia, Universidad Catolica del Norte, Av. Angamos 0610, Antofagasta Chile*
[3]*Pulkovo Observatory, Pulkovskoe Shosse 65, Saint-Petersburg 196140, Russia*
[4]*INAF – Osservatorio Astronomico di Cagliari, via della scienza 5-I-09047 Selargius, Italy*
[5]*INAF – Osservatorio Astronomico di Palermo, piazza Parlamento 1-I-90134 Palermo, Italy*

Accepted 2015 May 14. Received 2015 May 14; in original form 2015 February 20

ABSTRACT

The wavelength displacements of the diffuse interstellar bands (DIBs) at 4502, 5705, 5780, 6284 and 7224 Å, with respect to the well-known, narrow atomic/molecular interstellar lines (of Ca II and Na I), have been measured in the spectra of the two Orion Trapezium stars, HD 37022 and HD 37020, using the HARPS–N spectrograph, attached to the 3.5-m Telescopio Nazionale Galileo, and the Bohyunsan Optical Astronomy Observatory (BOAO) echelle spectrograph (BOES), attached to the 1.8-m Korean telescope. The redshift is ∼25 km s^{-1} for all these DIBs. We discuss the various possible origins of this very peculiar wavelength shift in the light of the particular physical conditions in the Orion Trapezium. The above-mentioned shift is seemingly absent in the DIBs at 6196 and 6993 Å.

Key words: line: identification – line: profiles – ISM: atoms – ISM: individual objects: θ Ori – ISM: lines and bands – ISM: molecules.

1 INTRODUCTION

The absorption spectra of interstellar clouds contain well-known molecular bands of simple polar radicals, CH, CN, CH^+, which were discovered and identified long ago (McKellar 1941). For a long time, they were believed to be the only possible interstellar molecules. In the 1970s, small homonuclear molecules (H_2, C_2) were also found. At the same time, rotational emission features revealed the presence – specifically in the dense interstellar medium (ISM), and mostly in star-forming regions – of many complex molecules with a dipole momentum. The full list of these polar species (mostly carbon-bearing) currently numbers more than 190 entries,[1] clearly demonstrating that a rich chemistry, mostly carbon-based, takes place in interstellar clouds. Some of these species have recently been observed in the middle and far-infrared by the space telescope *Herschel*. The largest currently known interstellar molecules are the fullerenes C_{60} and C_{70} (Cami et al. 2010; Berné, Mulas & Joblin 2013). Still unknown (unidentified) molecular species are believed to be the carriers of diffuse interstellar bands (DIBs), and these make up the longest-standing unsolved problem in astronomical spectroscopy. The first two DIBs were discovered in 1921 by Heger (1922). Until 1970, the list of DIBs was very short, with only nine entries. The use of solid-state detectors and more powerful telescopes for DIB observations led to the progressive discovery of many additional weak features, almost all of them in the range from the near-ultraviolet to the near-infrared. The current lists of known DIBs contain over 400 entries (Galazutdinov et al. 2000a; Hobbs et al. 2009), the majority of which are very shallow. Some of the weaker features are not unambiguously detected and are classified as DIBs in all surveys (e.g. Bondar 2012). Even more importantly, fine structures – reminiscent in some cases of the unresolved rotational envelopes of bands of polyatomic molecules – have been resolved in some DIBs (Kerr et al. 1998). Nearly all conceivable forms of matter, from the hydrogen anion to colour centres in dust grains, have already been proposed as DIB carriers. All of them have been rejected, with very few still tentative exceptions. Recently, Krełowski et al. (2010) found a very weak DIB, which coincides with an electronic, gas-phase band of HC_4H^+, supporting the molecular DIB origin. Linnartz et al. (2010) reported another coincidence between a lifetime-broadened absorption spectrum recorded through a hydrocarbon plasma and a strong DIB at 545 nm, but an unambiguous identification of the carrier has not yet been possible. Maier et al. (2011) were the first to propose l-C_3H_2, but this identification would imply that this species is surprisingly abundant in the ISM; moreover, another broad DIB, initially interpreted as a second l-C_3H_2 feature (from the same level) near 4883 Å clearly has a different origin (Krełowski, Galazutdinov & Kolos 2011). Two strong DIBs in the near-infrared were tentatively attributed to C_{60}^+ by Foing & Ehrenfreund (1994) on the basis of laboratory spectra measured in solid rare-gas matrices, but this

⋆ E-mail: jacek@astri.uni.torun.pl (JK); gmulas@oa-cagliari.inaf.it (GM); cecchi-pestellini@astropa.inaf.it (CCP)
[1] See, e.g. http://astrochymist.org/astrochymist_ism.html.

was disputed by Jenniskens et al. (1997) and Galazutdinov et al. (2000a). Despite the recent detection of the vibrational spectrum of C_{60}^+ (Berné et al. 2013), its identification or rejection as a DIB carrier still awaits gas-phase laboratory spectra, as yet unavailable. Similarly, Iglesias-Groth et al. (2008) and Iglesias-Groth, González Hernández & Manchado (2012) recently claimed to have identified the electronic transitions of gas-phase singly charged naphthalene, the simplest polycyclic aromatic hydrocarbon (PAH) in the spectra of Cernis 52 and, more recently, of HD 125241. In Cernis 52, a well-defined band is firmly detected, which is consistent with the strongest band of $C_{10}H_8^+$. Other, weaker, bands are compatible with observations, but their presence is not as firmly established, mainly due to stellar line contamination. In the case of HD 125241, the authors might have been misled by the fact that the spectrum of this star is populated with many stellar emission lines, possibly of circumstellar origin. One of these, centred at 6701.2 Å and due to Si IV, is very broad. Setting the continuum over the red wing of this emission could easily have created a broad depression as an artefact, where the authors identify the strongest naphthalene band. This has never been confirmed in any other sources, and no other features of this molecule have yet been firmly identified on the same source, being at best weak features superimposed on stronger stellar features contaminating them. Iglesias-Groth et al. (2010) also claimed to have identified a band of the anthracene cation ($C_{14}H_{10}^+$) in the spectrum of Cernis 52. However, this one band is obtained after subtraction of a stronger, very close, overlapping stellar feature, and no other bands of $C_{14}H_{10}^+$ were detected. It was furthermore rebutted by Galazutdinov et al. (2011), so that this claimed identification must be regarded as tentative. No other specific PAH features have been found, despite several dedicated efforts (e.g. Gredel et al. 2011; Salama et al. 2011).

After more than 90 yr of DIB research, despite having learned much about diffuse and translucent clouds, the identification of DIBs has still not been achieved. We emphasize that a vast majority of reddened stars have been observed through several translucent clouds. As a result, we observe DIBs in ill-defined averages – the physical parameters and spectra of individual clouds can be very different (Krełowski & Westerlund 1988). The fact that DIBs are most frequently observed through a number of possibly very different clouds is likely to be one of the reasons for their apparent uniformity, washing out individual differences. This conversely makes all 'peculiarities' very attractive, as the latter are most likely spectra of individual clouds, where the physical conditions might be more homogeneous than in a random sample of clouds. Thus, a more sensible, unambiguous physical interpretation of the spectra is possible. The examples of extreme peculiarities shown by Krełowski & Westerlund (1988) – namely σ Sco and ζ Oph – have become the archetypes of translucent interstellar clouds of evidently different spectra.

In this sense, objects belonging to the Orion OB1 association, a region of active star formation, were discovered to be among the most interesting. The stars forming the famous Orion Trapezium are quite substantially reddened, but the clouds obscuring these objects are very peculiar. Their extinction curves are very unusual (Fitzpatrick & Massa 2007) and the features carried by the simple radicals typically fall below the level of detection. Regarding the DIBs, only two very broad ones, at 5780 and 6284 Å, are strong with respect to extinction; those at 6196, 6205, 6010 and 5705 Å are detectable but weak (Krełowski & Greenberg 1999). Also, Krełowski & Greenberg (1999) found surprising redshifts for some DIBs in relation to the interstellar sodium doublet, the only evident atomic line clearly seen in the spectra of the Ori OB1 stars available at that time. This result was confirmed later by Walker et al. (2001), but only for HD 37061. Because the stability of the rest wavelengths of DIBs is one of their most well-established observational properties, this result is indeed extremely peculiar, and we therefore set out to further investigate it.

In this paper, we aim to confirm the above results and to relate the peculiar behaviour of DIBs to that of simple molecular species. The point is to use high-quality, high-resolution spectra from more than one instrument. The Ori OB1 association is the nearest region of active star formation and thus it is very interesting to consider what type of physical conditions might be caused by the proximity of clouds and young, hot stars and how these conditions might influence the formation of DIB carriers, DIB spectral profiles and wavelength shifts.

2 OBSERVATIONS

We have used the HARPS–N echelle spectrograph[2] (Cosentino et al. 2012), attached to the 3.5-m Telescopio Nazionale Galileo. It offers a resolution of $R = 115\,000$ in the spectra, divided into 70 orders. This resolution allows us to resolve Doppler components likely to be present in interstellar features, while the telescope size allows us to achieve a high signal-to-noise (S/N) ratio. Moreover, having been designed and built specifically for the main purpose of detecting exoplanets, measuring radial velocity variations via accurate determinations of Doppler shifts, HARPS–N has a very stable and reliable wavelength calibration.

In addition, to be able to rule out instrumental artefacts, we have also used the data of the same targets collected by the Bohyunsan Optical Astronomy Observatory (BOAO) echelle spectrograph[3] (BOES; Kim et al. 2007), attached to the 1.8-m telescope of the BOAO in Korea. This instrument can operate in three observational modes, providing resolving powers of 30 000, 45 000 and 90 000, respectively. Our spectra were taken using the highest resolving power, enabling us to observe relatively weak, narrow features. In all observational modes, the spectrograph records the whole spectral range from ∼3500 to ∼10 000 Å, divided into 75–76 spectral orders.

All of the data were reduced using IRAF[4] (Tody 1986) and the DECH data reduction suite, written and made available[5] by one of the authors (G. Galazutdinov). Data reduction involved the standard procedure of order location, bias and background subtraction, flat-fielding, extraction of one-dimensional spectra order by order, and wavelength calibration through comparison with a reference spectrum of a Th–Ar lamp. The accuracy of the wavelength calibration and the absence of instrumental effects, which can displace the final wavelength solution, were verified by the cross-correlation of the strong telluric bands present in all studied targets with a reference synthetic telluric spectrum.

The stars we have observed are HD 37022 and HD 37020 (both in the Orion Trapezium), HD 24398 as a reference 'normal DIB' star, and the bright unreddened star HD 22928, used as a telluric line divisor. Their basic data are given in Table 1.

[2] http://www.tng.iac.es/instruments/harps/
[3] http://www.boao.re.kr/BOES/BOESppt3.files/frame.htm
[4] IRAF is distributed by the National Optical Astronomy Observatories, which are operated by the Association of Universities for Research in Astronomy, Inc., under cooperative agreement with the National Science Foundation.
[5] http://www.gazinur.com/DECH-software.html

Table 1. Target list with basic stellar data (from the SIMBAD data base, Wenger et al. 2000).

HD number	RA	Dec.	l	b	Sp. type	V (mag)	$E(B-V)$	$v_{\rm rad}$ (km s^{-1})
22928	03 42 55.504	+47 47 15.17	150.2834	−05.7684	B5 IIIC	3.01	0.00	4.0
24398	03 54 07.922	+31 53 01.08	162.2891	−16.6904	B1 Ib	2.85	0.31	20.6
37020	05 35 15.829	−05 23 14.36	209.0072	−19.3853	B0.5 V	6.73	0.26	28.3
37022	05 35 16.464	−05 23 22.85	209.0107	−19.3841	O7 V	5.13	0.31	23.6

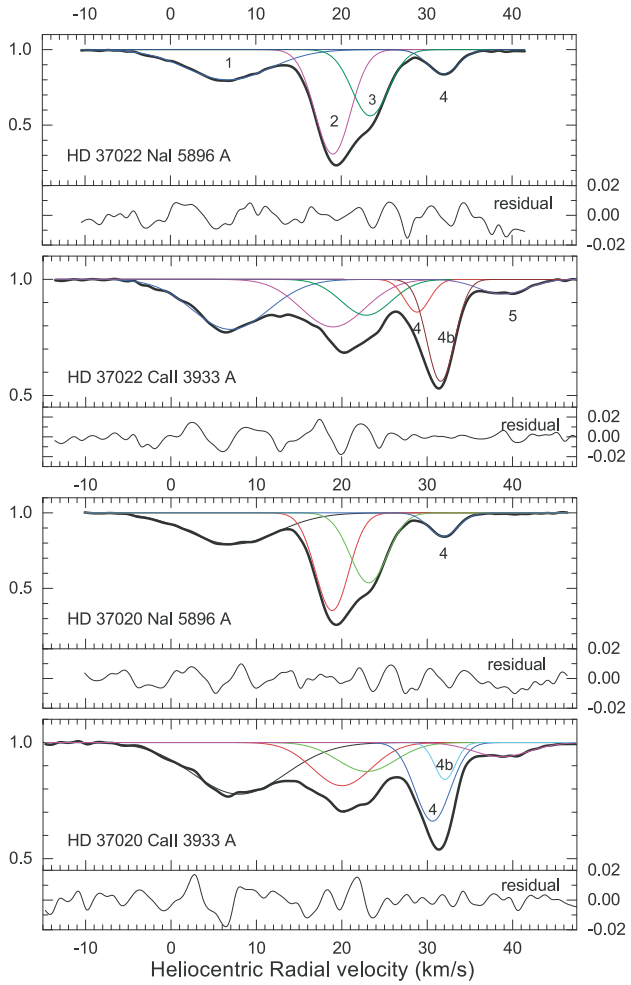

Figure 1. Doppler structure of the atomic lines of Ca II and Na I lines, in radial velocity scale, for HD 37022 (top panel) and HD 37020 (bottom panel). In each spectrum, the thick black line is the normalized observed flux, the thin coloured lines are individual fitted components, and the residual (difference between observation and fitted model) is shown at the bottom. Components are labelled in the Figure matching the identifications in Table 2.

3 RESULTS

HARPS–N allows very accurate and reliable determinations of wavelengths and this is why we have used it in this project. The range covered by the spectrograph (3855–6910 Å) includes two prominent doublets of Ca II and Na I that are usually very strong. The Orion Trapezium stars are also known to exhibit strong nebular emission lines (e.g. Baldwin et al. 2000), apparently originating in the close vicinities of the observed stars. This spectrograph is thus very well suited to check whether the redshift of some DIBs reported by Krełowski & Greenberg (1999) can be confirmed.

Fig. 1 shows an enlarged view of the two atomic lines of Na I at 5896 Å and Ca II at 3933 Å, in heliocentric radial velocity scale, for the Orion trapezium stars HD 37020 and HD 37022. These stars are separated by less than 13 arcsec, and indeed the lines of sight towards both of them appear to traverse very nearly the same foreground ISM, showing almost identical components with the same radial velocities and equivalent widths. Not unusually, while both Na I and Ca II show matching components at almost the same radial velocities, the intensity ratios are different and their respective absolute maxima are in different radial velocity components.

Table 2. Heliocentric radial velocity components measured in the Na I line at 5896 Å and Ca II line at 3933 Å in the two Orion Trapezium stars HD 37022 and HD 37020. Radial velocities are given in km s^{-1}, and their errors are less than 0.5 km s^{-1}. Equivalent widths (EWs) are in mÅ.

		Radial velocity (EW)	
		HD 37022	HD 37020
Comp. 1	Na I	6.8 (48.7 ± 1.3)	7.2 (52.6 ± 1.8)
	Ca II	7.0 (31.7 ± 0.9)	8.0 (39.74 ± 1.3)
Comp. 2	Na I	19.0 (70.4 ± 0.6)	18.7 (61.8 ± 0.7)
	Ca II	19.0 (25.2 ± 0.8)	20.0 (20.8 ± 1.1)
Comp. 3	Na I	23.4 (46.0 ± 0.6)	23.1 (49.6 ± 0.8)
	Ca II	22.8 (14.9 ± 0.7)	22.9 (13.9 ± 0.8)
Comp. 4	Na I	31.9 (14.2 ± 0.5)	31.9(13.0 ± 0.6)
	Ca II	28.8 (6.7 ± 0.3)	30.6 (22.8 ± 0.5)
Comp. 4b	Ca II	31.6 (23.4 ± 0.4)	32.1 (6.4 ± 0.3)
Comp. 5	Na I	–	–
	Ca II	38.8 (5.9 ± 0.6)	38.7 (6.6 ± 0.7)

Table 2 lists the measured components, in both Na I and Ca II lines. In Ca II, it was necessary to use two Gaussians around ∼30 km s^{-1} to account for the slightly asymmetric profile of this velocity component. Only one Gaussian was necessary to fit the matching velocity component of Na I. The velocity component at ∼40 km s^{-1} could only be detected in the Ca II line. The uncertainty of radial velocities was estimated by examining the differences between values measured for the same components in the two lines of the Na I and Ca II doublets, respectively.

Fig. 2 unambiguously shows the redshift of the 5780-Å DIB using the HARPS–N spectra. We used the HD 24398 star as a reference 'normal DIB' object. The latter is known as an object in which all interstellar lines are dominated by a heliocentric Doppler velocity of about 14 km s^{-1} (Bondar 2012), with some structure barely detectable only at extremely high resolution and S/N ratio. Welty, Morton & Hobbs (1996) resolved eight components for Ca II with radial velocities between −6 and 22 km s^{-1}, but with ∼80 per cent of the estimated column density being within the range 13–16 km s^{-1}. From this figure, it is apparent that the maximum of the 5780-Å DIB in HD 37022 is not found at its expected wavelength, but instead it is redshifted by ∼0.58 Å, corresponding to a Doppler shift of about

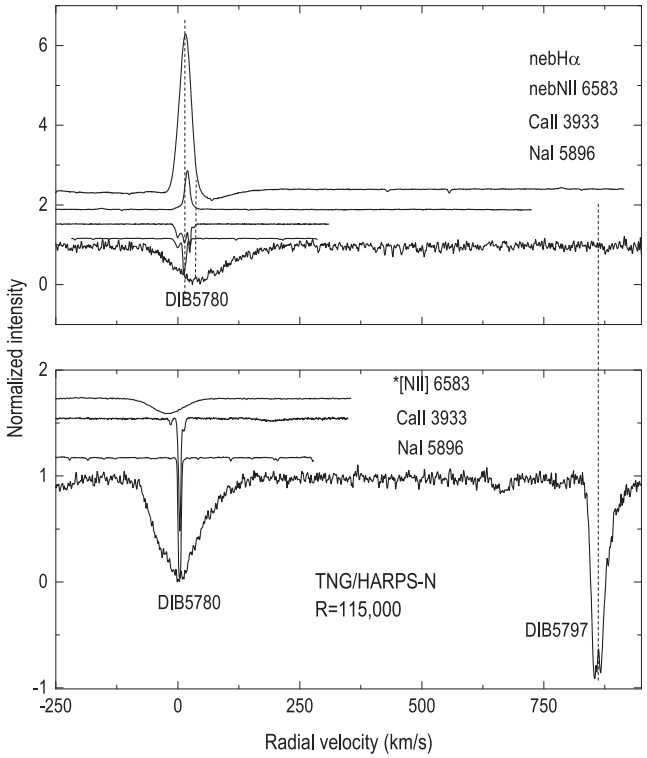

Figure 2. The top panel shows the strongest DIB at 5780 Å in the spectrum of HD 37022, shown in radial velocity scale together with other interstellar and nebular lines. The zero in the velocity scale is chosen to coincide with the strongest component visible in the D_1 Na I line. All spectra have been normalized to the continuum, and shifted for clarity. The ordinate scale is arbitrary. The two dashed lines mark the position of the zero velocity component and the position of the peak of the 5780-Å DIB, clearly redshifted by ∼30 km s^{-1}. A similar plot is also shown in the bottom panel for the reference star HD 24398; this object shows no detectable nebular lines. The 5780-Å DIB appears in this case (as in almost all cases) to be perfectly aligned (within ∼2 km s^{-1}) with interstellar atomic features.

30 km s^{-1} with respect to the radial velocity of peak absorption in Na I. While the Doppler structure of the Ca II line shows some redshifted components, the redshift we measured for the 5780-Å DIB goes clearly beyond it, where no atomic absorption component was detected. Less evidently, but measurably, the 5780-Å DIB in HD 37022 is also broader than in HD 24398, by about the same amount.

In the spectrum of HD 37022, we can also detect some nebular emission lines, likely to arise from the H II region around the same star. The Hα and two forbidden N II lines seen in emission appear to have a Doppler redshift of only a few km s^{-1} with respect to the strongest component of the Na I lines, in any case well within the velocity range spanned by the Doppler structure of the Ca II lines. The Hα appears to have a small Doppler shift, a few km s^{-1}, with respect to the N II lines. This agrees with previous studies of the nebular emission from the Orion Trapezium (Baldwin et al. 2000). Indeed, Baldwin et al. (2000) also found much larger velocity differences among nebular lines due to different species in different ionization states, suggesting that they arise from different parts of an accelerating wind. Because our observations are centred on the trapezium stars, fainter nebular lines are barely detectable in our spectra, and thus we cannot confirm this.

The Hα line also shows a superimposed, much broader absorption line. Its width hinders an accurate measurement of its radial velocity. A similar structure, namely an emission line with an underlying, much broader absorption line, can be seen in Hβ. In Hβ, the absorption component is stronger, and it can be seen to be approximately aligned with the radial velocity of the emission component. Upon checking the radial velocity of a few photospheric lines on our HARPS–N data (e.g. N III at 4003.6 Å, He I at 4026.2 Å, C III at 4162.9 Å, Si IV at 4212.4 Å, O II at 4366.9 Å, O III at 5508.1 Å and C IV at 5812.0 Å), they appear consistent with the most current value found in the literature (∼23.6 km s^{-1}; Olivares et al. 2013), even if there is some scatter between different lines, at the level of less than ∼2 km s^{-1}. This scatter might be due to the documented variability of stellar lines in HD 37022, attributed to the complex interplay of its magnetic field, fast wind and some infalling material (Simón-Díaz 2006; Wade et al. 2006). This is mostly apparent when comparing, for example, the N III line at 4003.578 Å and the He I line at 4009.258 Å: the Doppler shift of the former corresponds to a heliocentric radial velocity of about 9.5 km s^{-1} while for the latter the value is about 41 km s^{-1}. However, the vast majority of the observed stellar lines is consistent with a radial velocity of 22–23 km s^{-1}.

We have not included HD 37020 in Fig. 2 because it is almost indistinguishable from that of HD 37022, just with very slightly weaker DIBs and lower S/N ratio, and hence it would not add any additional information here (see Fig. 3).

Fig. 3 shows a comparison of the DIBs that can be measured in HD 37020, HD 37022 and the reference star HD 24398 with HARPS–N, again in radial velocity scale, using the Doppler shift of the strongest component of the D_1 Na I line in the same spectrum as reference. Four of the five DIBs shown, the relatively broad bands, are clearly redshifted in HD 37020 and HD 37022 with respect to the D_1 Na I line marking the zero of the velocity scale. Their shift is compatible with a unique relative radial velocity, and all of them also exhibit a similar broadening with respect to the DIBs measured in the reference star HD 24398. Remarkably, the peak of the narrow 6196-Å DIB in HD 37020 and HD 37022 appears to be perfectly aligned (within ∼5 km s^{-1}) with the Doppler velocity of the atomic lines. The ratio of DIB intensity is also evidently different between HD 37022 and HD 24398: in the former, the 6284-Å DIB is stronger than the 5780-Å DIB, while the reverse happens in the latter. Moreover, a weak, narrow DIB at 6287 Å appears on the red wing of the 6284-Å DIB in HD 24398, which is below the level of detection in HD 37022.

To further strengthen the fact that the observed redshift is not an (unlikely) instrumental artefact of HARPS–N, Fig. 4 shows the 5780- and 6196-Å DIBs observed in HD 37022 with the BOES at slightly lower spectral resolution (90 000 versus 115 000), which precisely match (within ∼1 km s^{-1}) the HARPS–N data. In addition, Fig. 4 shows two more DIBs that are out of the spectral range covered by HARPS–N, namely the 6993- and 7224-Å DIBs. The peak of the former, relatively narrow, precisely matches (within ∼1 km s^{-1}) the Doppler shift of the D_1 Na I line, like the 6196-Å DIB. The 7224-Å DIB, conversely, a relatively broad band, again appears redshifted like the 5780-Å DIB.

For a solid quantitative measurement of the radial velocity shifts visually apparent in Figs 2, 3 and 4, we used the same method commonly used to precisely measure the radial velocities of stars, correlating their observed spectra with a template (see for example, Queloz 1995, and references therein). We performed the correlation analysis one DIB at a time, using as a template the DIB profiles measured in HD 24398. This measurement is not coincident with velocity shifts measured using DIB peaks as a reference, nor is it expected to be: the correlation yields velocity shifts between

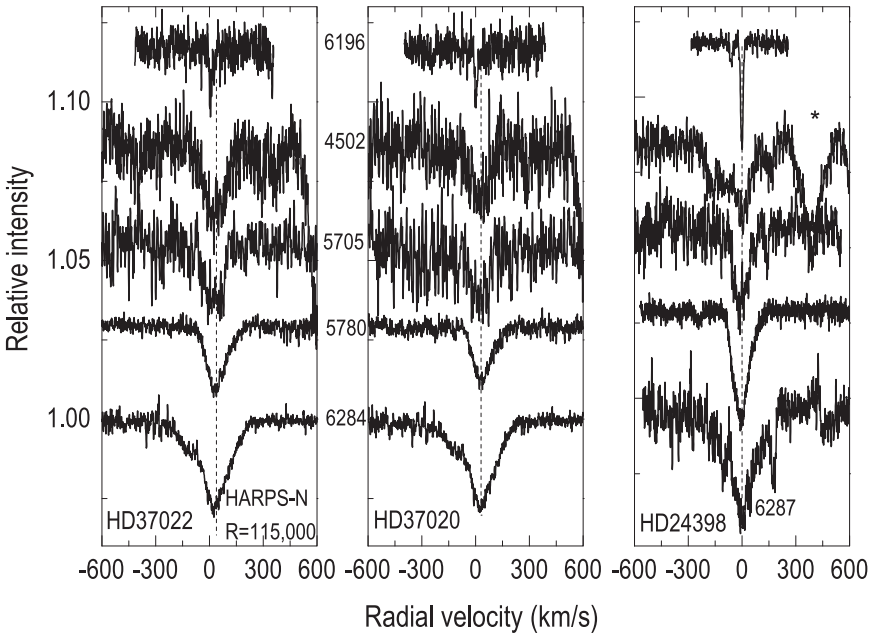

Figure 3. Five diffuse bands observed in the HARPS–N spectrum of θOri (left and middle panels) and, for reference, of ζPer (right panel). To ease the comparison of their radial velocities, all DIBs were scaled to the same maximum intensity. All bands have been referred to the peak absorption in Na I lines (see Fig. 2). Four of them (the relatively broad bands) show a very similar redshift in θOri. The fifth band (at 6196 Å) is either not redshifted at all or the shift is below the level of detection.

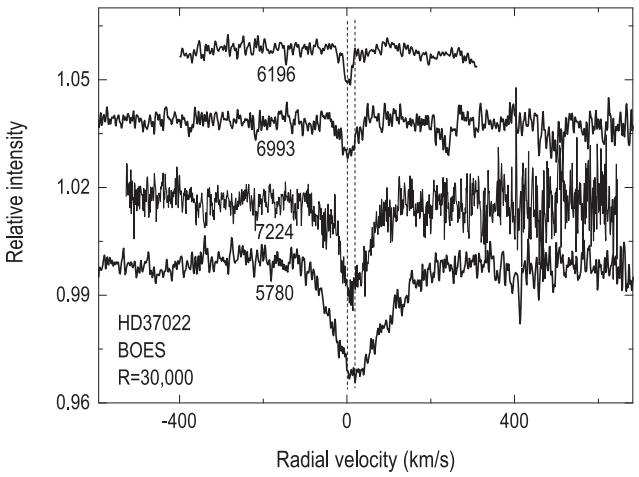

Figure 4. Four DIBs from the BOES spectra of HD 37022, including two not measurable with HARPS–N. The narrow 6993-Å feature is evidently unshifted, like the 6196-Å DIB, while the broad 7224-Å DIB shares the same redshift as the 5780-Å DIB.

feature centroids, which would coincide with shifts measured on the peaks only in case of infinite S/N ratio and perfectly identical spectral shapes between spectrum and correlation template. Most DIBs are detectably broader in the Orion Trapezium with respect to HD 24398, and noise is clearly far from negligible. Remarkably, the only two narrow DIBs, for which the radial velocity shift thus determined is most significant and least sensitive to the determination method, are compatible with zero radial velocity relative to the interstellar rest frame given by the strongest components in the Na I D_1 and CH 4300 Å lines. This correlation procedure, as implemented in the DECH and IRAF data reduction software, yields the radial velocities maximizing the correlation and their standard deviations, via R-statistics analysis. The results are listed in Table 3.

Table 3. Radial velocity displacement (in km s^{-1}) of the DIBs, obtained by correlating their spectra in the Orion Trapezium stars with the reference spectra observed towards HD 24398. Radial velocities for the Trapezium stars are referred to the strongest D_1 line component, assumed to mark the interstellar rest frame. For HD 24398, the interstellar rest frame is assumed to coincide with the radial velocity of the molecular CH 4300-Å line. The listed rest wavelengths for the diffuse bands are from Galazutdinov et al. (2000b).

DIB (Å)	HD 37022 (km s^{-1})	HD 37020 (km s^{-1})
4501.80	$+25 \pm 10$	$+30 \pm 10$
5705.20	$+28 \pm 5$	$+33 \pm 5$
5780.37	$+24 \pm 1$	$+23 \pm 1$
6195.97	$+3 \pm 4$	$+6 \pm 5$
6283.85	$+20 \pm 1$	$+22 \pm 1$
6993.18	-1 ± 5	n/a
7223.91	$+27 \pm 1$	n/a

4 DISCUSSION AND CONCLUSIONS

The redshift of the DIBs at 4502, 5705, 5780, 6284 and 7224 Å observed in HD 37022 can be interpreted in two different ways: (i) the peculiar physical conditions along, or around, HD 37022 produce intrinsically different DIB profiles, broader and peaking at a different position; (ii) the observed DIBs are produced by Doppler structure, as possibly hinted by all shifted DIBs sharing (or compatible with) the same redshift and broadening in velocity scale.

To test the feasibility of the latter hypothesis, we attempted a conditioned least-squares fit of the redshifted 5780- and 6284-Å DIBs in HD 37022 with a superposition of two template DIBs (i.e. the ones observed in HD 24398). Therefore, the DIB as observed in HD 24398 was assumed as the intrinsic profile, and several copies of it with different scalings and Doppler shifts were used to fit the profile observed in HD 37022. The fit was constrained to only two Doppler components, one fixed at the Doppler velocity of the Na I lines, the other free to vary. The free parameters of the fit are therefore only three (for each DIB): the two intensities of the components (constrained to be positive) and the Doppler velocity of the redshifted component. We used the well-known Levenberg–Marquardt method (Levenberg 1944), as implemented in the MPFIT package (Markwardt 2009)[6] for IDL. This algorithm strives to numerically reduce the χ^2 computed between model and data, iteratively modifying an initial guess for the values of the free parameters, until a minimum is found. It is therefore possible to fall into local minima, especially with noisy data, and the solution found will, in this case, depend on the initial starting point. When several minima exist, they will normally have different χ^2 values, and some can be rejected on the sole basis of this. However, it might be that more than one solution has an acceptable χ^2 value; in this case, some of these can be rejected because the residual (difference between model and data) is clearly not white noise (i.e. with the model falling systematically below the data in some section of the spectrum and above it in another). This does happen with our fit here, with several solutions being in principle acceptable on the basis of χ^2 alone, but with only the best one (i.e. the one with the absolute minimum χ^2 value) producing a residual of white noise, with uncorrelated adjacent values. To make the determination of the acceptable fit more robust and less subjective, we filtered both the HD 37022 and the template DIBs with a mild smoothing filter (Fourier five-point filter as implemented in the DECH data reduction suite). This is justified by the fact that HARPS–N spectra are oversampled and the DIBs being fitted are intrinsically broad. When using the filtered data, only one acceptable solution is found, which corresponds to the absolute minimum of χ^2, while the unphysical ones are no longer even local minima. The resulting, very satisfactory best fits for the 5780- and 6284-Å DIBs are shown in Figs 5 and 7 for HD 37022 and Figs 6 and 8 for HD 37020.

In all cases, the residual between the fit and the original spectrum is essentially white noise, except for the obvious absence of the narrow DIB at 6287 Å in HD 37022, which is instead present in the reference HD 24398 spectrum and thus appears as an artefact in the residual in Fig. 7. When slightly smoothed spectra are used for the fit, the solution is very robust for both the 5780- and 6284-Å DIBs. In both cases, the additional fitted component is redshifted with respect to the interstellar sodium by $34 \leq v_{\rm add} \leq 40$ km s^{-1}, the best solution being $\sim$35 km s^{-1}. When the same fitting procedure is applied to the 5780- and 6284-Å DIBs in HD 37020, due to the lower S/N ratio, the solution is not unique even after smoothing, but all acceptable solutions nonetheless yield $34 \leq v_{\rm add} \leq 40$ km s^{-1} for the radial velocity of the additional component, consistent with what was found for HD 37022. These results can be compared to the radial velocity shifts listed in Table 3. However, because the latter were determined by correlation with a template consisting of a single component, for a meaningful comparison we must compare them with the weighted average of the radial velocities of the two components of the fit performed here, the weights being their relative intensities. This results in very nearly the same numbers of

[6] http://purl.com/net/mpfit

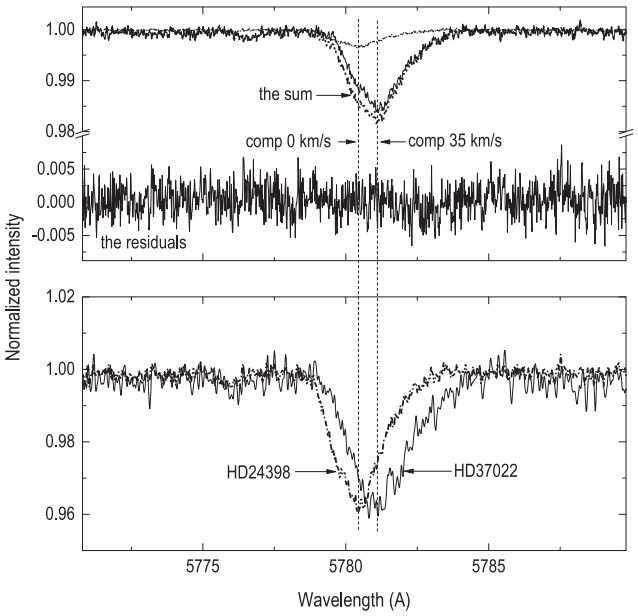

Figure 5. Upper panel: the 5780-Å DIB profile in HD 37022, fitted with the composition of two profiles identical to that of HD 24398. The radial velocity difference is 35 km s^{-1}. Lower panel: profile difference between the standard reference one of HD 24398 and the one observed in HD 24398, both normalized to the same peak depth and referred to the reference frame given by the radial velocity of the peak absorption in the Na I atomic lines observed in their respective spectra.

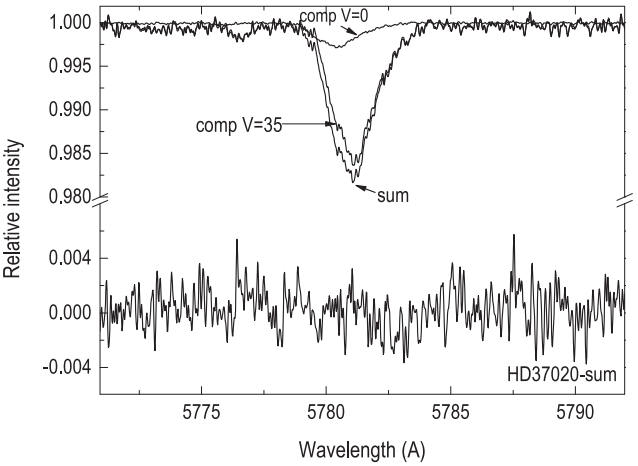

Figure 6. The 5780-Å DIB profile in HD 37020, fitted with the composition of two profiles identical to that of HD 24398 (same as the upper panel in Fig. 5). The radial velocity difference is the same, namely 35 km s^{-1}.

Table 3 for the DIBs at 5780 and 6284 Å. The noise in the other DIBs in HD 37022 and HD 37020 is so high that the fits are not robust (i.e. many equivalently acceptable fit solutions are found) but they are compatible with the results found for the 5780- and 6284-Å DIBs (i.e. $v_{\rm add} \sim 35$ km s^{-1} is always one of the acceptable solutions of the fit). Therefore, while we do not claim that this is the only possible interpretation of the data, we do find it to be possible and self-consistent.

Of course, this then raises more questions. What is producing the redshifted component of the DIBs? Is it some residual, still infalling material of the young, newly formed, very early-type stars, or does

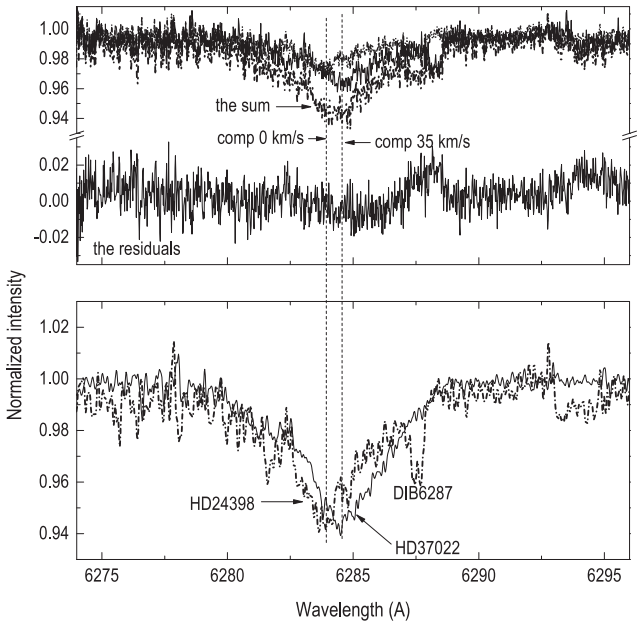

Figure 7. Same as in Fig. 5, but for the 6284-Å DIB. The radial velocity difference between the two components is the same, namely 35 km s^{-1}. Note the presence, only in HD 24398, of the narrow 6287-Å DIB.

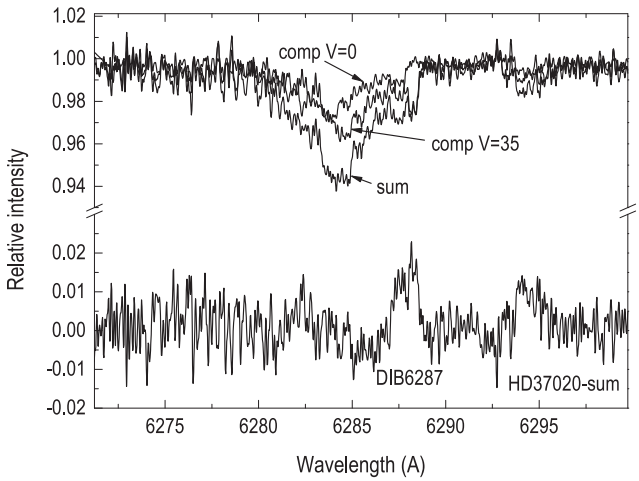

Figure 8. The 6284-Å DIB profile in HD 37020, fitted with the composition of two profiles identical to that of HD 24398 (same as the upper panel in Fig. 7). The radial velocity difference is the same, namely 35 km s^{-1}.

it arise in the evaporating layer of the photodissociation region, at the edge of the H II region? Why is this additional Doppler component not detected in atomic lines? Upon comparing the Doppler structures of the Na I and Ca II lines in Fig. 1 and Table 2, there appears to be a temperature gradient with increasing radial velocities, whereby Na I lines decrease while Ca II increases, and the highest velocity component is detected only in Ca II, but it is weaker. Therefore, there might be another, more redshifted component with a still higher temperature, in which sodium and singly ionized calcium are absent, but this is difficult to assess with the available data. Observations with a substantially higher S/N ratio would enable us to perform a robust fit on the other three redshifted DIBs. It is clear that if five different DIBs were robustly consistent with the same Doppler structure, yielding the same radial velocity as the only acceptable fit for the additional component of all of them, this would provide to be solid evidence for this interpretation. Conversely, if each DIB were found to require a different radial velocity structure, this would make this interpretation just a pointless mathematical exercise. Furthermore, a substantially higher S/N ratio might also enable us to detect either additional Doppler components in sodium and calcium lines, or weak molecular features (CH, CH^+, CN), which are below the detection limit in current data. This would also be extremely interesting because there is some observational evidence that, for example, CH, CH^+ and CN features do not always show all the same Doppler components, with CH^+ features sometimes shifted with respect to the other species and to atomic lines (see for example, Allen 1994).

As to the other possible interpretation (i.e. different intrinsic profiles of the redshifted DIBs in HD 37022), this is tempting in the light of the recent observations of Herschel 36 (Oka et al. 2014a,b; York et al. 2014). In this extremely peculiar line of sight, CH and CH^+ were observed to have an anomalously high rotational temperature, and some DIBs were simultaneously found to be anomalously broad (much more than we observe here), with a very wide red wing, and the peaks of some of them slightly redshifted (less than we observe here). This has been tentatively interpreted as unresolved rotational envelopes of molecular bands, which in Herschel 36 appears to have an anomalously high rotational excitation. If this were the correct interpretation for HD 37022, then this would be an intermediate case between the standard excitation conditions of the cold neutral ISM, where normal DIBs arise, and those prevailing in Herschel 36. However, the DIB at 5797 Å is prominent, and prominently broadened, in Herschel 36, and instead is undetectable in HD 37022; also, the 6196-Å DIB is one of the broadened bands in Herschel 36, while no such effect is evident in our data of HD 37022 (but some limited broadening might be consistent with our observations, hidden by the noise). Also, the 6284-Å DIB is broadened but not redshifted in Herschel 36, while it is redshifted in HD 37022. To test this hypothesis, again it would be useful to obtain deeper observations with higher S/N ratio, to detect CH, CH^+ and CN features, to determine their rotational temperatures in HD 37022 and to explore their relations with the observed profiles and positions of redshifted DIBs. We remark that HD 37022 and Herschel 36 also have peculiar extinction curves (Fitzpatrick & Massa 2007), hinting that dust properties are also unusual. Actually, Herschel 36 appears to be a tight triple system (Arias et al. 2010; Sanchez-Bermudez et al. 2014). Fitzpatrick & Massa (2007) give it the spectral classification of the third, most luminous, O7.5 V type star of the system, which certainly dominates the *International Ultraviolet Explorer* spectrum they used to derive the extinction. The spectrum in the visible, in which the peculiar DIBs were observed, contains non-negligible contributions from all three unresolved stars. In any case, the extinction curve and DIBs are very likely to be extremely similar for all three stars of such a close system, unless circumstellar material makes a large contribution to them.

Fig. 9 shows the extinction curves reported by Fitzpatrick & Massa (2007) for HD 37020, HD 37022 and Herschel 36, together with the fits of such curves with the $[CM]^2$ dust model, as reported in Mulas et al. 2013. For comparison, Fig. 10 shows the extinction curve of HD 23180 (o Per), the closest proxy of HD 24398 (ζ Per) available in the sample of Fitzpatrick & Massa (2007), and the average galactic one. The macroscopic dust component appears to be very similar for all three stars in Fig. 9, all very different from the reference stars in Fig. 10. Upon examining tables 4 and 5 in Mulas

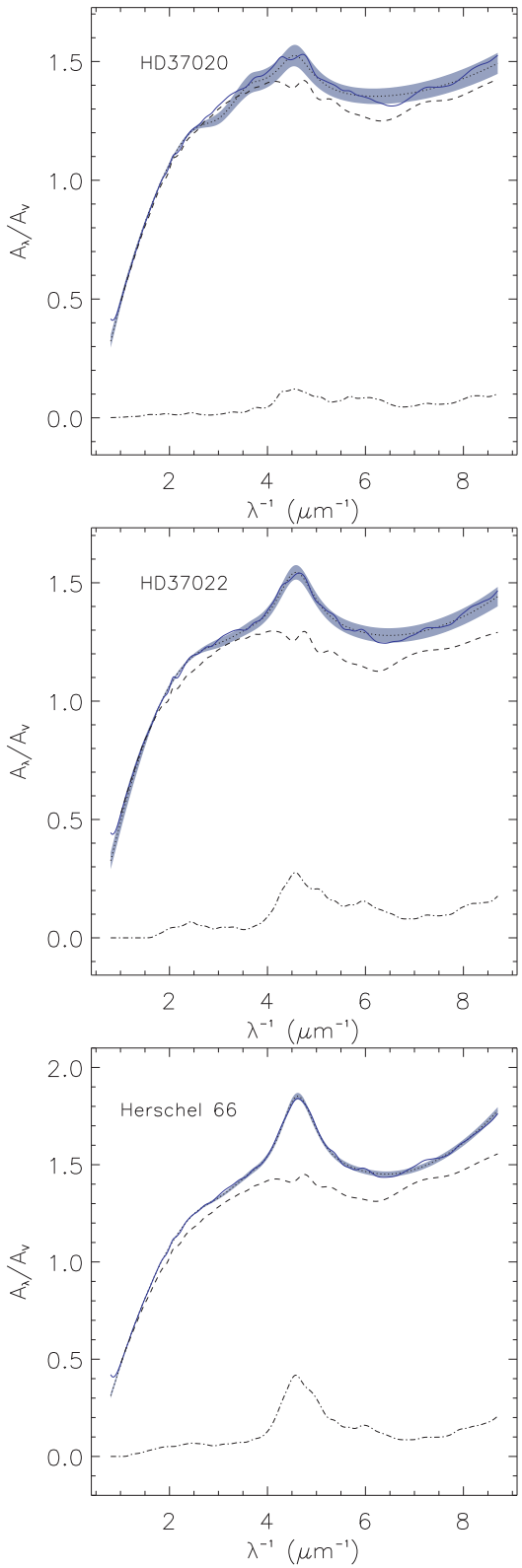

Figure 9. Extinction curves of HD 37020, HD 37022 and Herschel 36. The dotted lines are the observations by Fitzpatrick & Massa (2007) and the shaded area represents the error estimated by the authors. The continuous lines represent the best fit with the $[CM]^2$ model (Mulas et al. 2013), the dashed lines denote the contribution by macroscopic dust and the dash-dotted lines show the contribution by PAHs (Mulas et al. 2013).

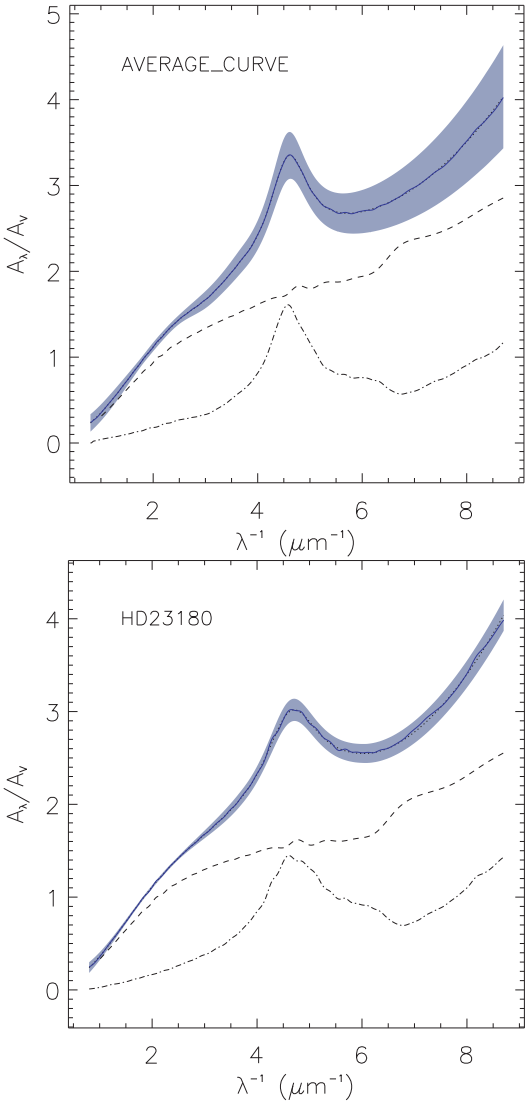

Figure 10. Same as Fig. 9, but for the average Galactic extinction curve and HD 23180 (o Per), another star in the same association as HD 24398 (ζ Per), likely to have a very similar extinction curve.

et al. (2013), we see that in all three cases, upon comparison with the galactic average and HD 23180, the dust population is dominated by large silicate grains, covered by a thick mantle of heavily processed (entirely, or almost entirely, aromatic) carbonaceous material. PAHs are very underabundant in all of them with respect to the HD 23180, our reference line of sight, similar to the galactic average. In the evolutionary scenario put forward by Cecchi-Pestellini et al. (2014), all three lines of sight appear to be composed of old, heavily processed dust.

It is unclear whether both DIBs and the extinction curves are made peculiar by some common physical cause related to the environment, or whether DIBs might be altered due to particular dust properties. Redshift and broadening in molecular electronic bands are commonly caused by attachment of molecules to a solid substrate (see for example, Tielens & Allamandola 1987). In an environment apparently devoid of small dust particles and PAHs (Mulas et al. 2013), in which apparently smaller nanograins and macromolecules are either destroyed or coalesce on to larger ones,

possibly some DIB carriers can also partially attach to grain surfaces, producing what we observe in HD 37022.

Clearly, a strategy to pursue in order to try to find the cause of the redshift of some DIBs in HD 37022, besides obtaining better observations of HD 37022 and valid regardless of the interpretation, would be to find other similar cases, to understand what they have in common and thus what makes them different from the standard cases. Selecting lines of sight for further DIB observations and choosing those with peculiar extinction curves similar to that of HD 37022 (Fitzpatrick & Massa 2007) might be the key in this respect.

ACKNOWLEDGEMENTS

This paper includes data gathered with the 3.5-m Telescopio Nazionale Galileo, and data collected with the 1.8-m telescope at the BOAO (South Korea). JK acknowledges the financial support of the Polish National Center for Science during the period 2012–2015 (grant UMO-2011/01/BST2/05399). GAG acknowledges the support of the Chilean fund FONDECYT-regular (project 1120190). GM and CCP acknowledge the support of the Autonomous Region of Sardinia, Project CRP 26666 (Regional Law 7/2007, Call 2010).

REFERENCES

Allen M. M., 1994, ApJ, 424, 754
Arias J. I. et al., 2010, ApJ, 710, 30
Baldwin J. A., Verner E. M., Verner D. A., Ferland G. J., Martin P. G., Korista K. T., Rubin R. H., 2000, ApJS, 129, 229
Berné O., Mulas G., Joblin C., 2013, A&A, 550, L4
Bondar A., 2012, MNRAS, 423, 725
Cami J., Bernard-Salas J., Peeters E., Malek S. E., 2010, Sci, 329, 1180
Cecchi-Pestellini C., Casu S., Mulas G., Zonca A., 2014, ApJ, 785, 41
Cosentino R. et al., 2012, Proc. SPIE, 8446, 1
Fitzpatrick E. L., Massa D., 2007, ApJ, 663, 320
Foing B. H., Ehrenfreund P., 1994, Nat, 369, 296
Galazutdinov G. A., Krełowski J., Musaev F. A., Ehrenfreund P., Foing B. H., 2000a, MNRAS, 317, 750
Galazutdinov G. A., Musaev F. A., Krełowski J., Walker G. A. H., 2000b, PASP, 112, 648
Galazutdinov G. A., Manico G., Pirronello V., Krełowski J., 2004, MNRAS, 355, 169
Galazutdinov G. A., Lee B-C., Song I-O., Kazmierczak M., Krełowski J., 2011, MNRAS, 412, 1259
Gredel R., Carpentier Y., Rouillè G., Steglich M., Huisken F., Henning T.., 2011, A&A, 530, 26
Heger M. L., 1922, Lick Obs. Bull., 10, 141
Hobbs L. M. et al., 2009, ApJ, 705, 32
Iglesias-Groth S., Manchado A., García-Hernandez D. A., González Hernández J. I., Lambert D. L., 2008, ApJ, 685, 55
Iglesias-Groth S., Manchado A., Rebolo R., González Hernández J. I., García-Hernández D. A., Lambert D. L., 2010, MNRAS, 407, 2157
Iglesias-Groth S., González Hernández J., Manchado A., 2012, MNRAS, 420, 2785
Jenniskens P., Mulas G., Porceddu I., Benvenuti P., 1997, A&A, 327, 337
Kerr T. H., Hibbins R. E., Fossey S. J., Miles J. R., Sarre P. J., 1998, ApJ, 495, 941
Kim K-M. et al., 2007, PASP, 119, 1052
Krełowski J., Greenberg J. M., 1999, A&A, 346, 199
Krełowski J., Westerlund B. E., 1988, A&A, 190, 339
Krełowski J., Beletsky Y., Galazutdinov G. A., Kolos R., Gronowski M., LoCurto G., 2010, ApJ, 714, L64
Krełowski J., Galazutdinov G., Kolos R., 2011, ApJ, 735, 124
Levenberg K., 1944, Quarterly of Applied Mathematics, 2, 164
Linnartz H., Wehres N., van Winckel H., Walker G. A. H., Bohlender D. A., Tielens A. G. G. M., Motylewski T., Maier J. P., 2010, A&A, 511, L3
Maier J., Walker G. A. H., Bohlender D. A., Mazzotti F. J., Raghunandan R., Fulara J., Garkusha I., Nagy A., 2011, ApJ, 726, 41
Markwardt C. B., 2009, in Bohlender D. A., Durand D., Dowler P., eds, ASP Conf. Ser. Vol. 411, Astronomical Data Analysis Software and Systems XVIII. Astron. Soc. Pac., San Francisco, p. 251
McKellar A., 1941, PASP, 53, 233
Mulas G., Zonca A., Casu S., Cecchi-Pestellini C., 2013, ApJS, 207, 7
Oka T., Welty D. E., Johnson S., York D. G., Dahlstrom J., Hobbs L. M., 2014a, in Cami J., Cox N. L. J., eds, Proc. IAU Symp. 297, The Diffuse Interstellar Bands. Kluwer, Dordrecht, p. 94
Oka T., Welty D. E., Johnson S., York D. G., Dahlstrom J., Hobbs L. M., 2014b, ApJ, 773, 42
Olivares J., Sánchez L. J., Ruelas-Mayorga A., Allen C., Costero R., Poveda A., 2013, AJ, 146, 106
Queloz D., 1995, in Philip A. G. D., Janes K. A., Upgren A. R., eds, Proc. IAU Symp. 167, New Developments in Array Technology and Applications. Kluwer, Dordrecht, p. 221
Salama F., Galazutdinov G. A., Krełowski J., Biennier L., Beletsky Y., Song I-O., 2011, ApJ, 728, 154
Sanchez-Bermudez J., Alberdi A., Schödel R., Hummel C. A., Arias J. I., Barbá R. H., Maíz Apellániz J., Pott J.-U., 2014, A&A, 572, L1
Simón-Díaz S., Herrero A., Esteban C., Najarro F., 2006, A&A, 448, 351
Tielens A. G. G. M., Allamandola L. J., 1987, in Hollenbach D. J., Thronson H. A. Jr, eds, Astrophysics and Space Science Library Vol. 134, Interstellar Processes. Springer-Verlag, Berlin, p. 397
Tody D., 1986, Proc. SPIE, 627, 733
Wade G. A., Fullerton A. W., Donati J.-F., Landstreet J. D., Petit P., Strasser S., 2006, A&A, 451, 195
Walker G. A. H., Webster A. S., Bohlender D. A., Krełowski J., 2001, ApJ, 561, 272
Welty D. E., Morton D. C., Hobbs L. M., 1996, ApJS, 106, 533
Wenger M. et al., 2000, A&AS, 143, 9
York D. G. et al., 2014, in Cami J., Cox N. L. J., eds, Proc. IAU Symp. 297, The Diffuse Interstellar Bands. Kluwer, Dordrecht, p. 89

This paper has been typeset from a TEX/LATEX file prepared by the author.